UCRL- 91642
PREPRINT



# TIME-IMPLICIT SIMULATION OF PARTICLE-FLUID SYSTEMS

J. Denavit

This paper was prepared for presentation at
International School for Space Simulations,
Kauai, Hawaii, February 3-15, 1985

January 17, 1985

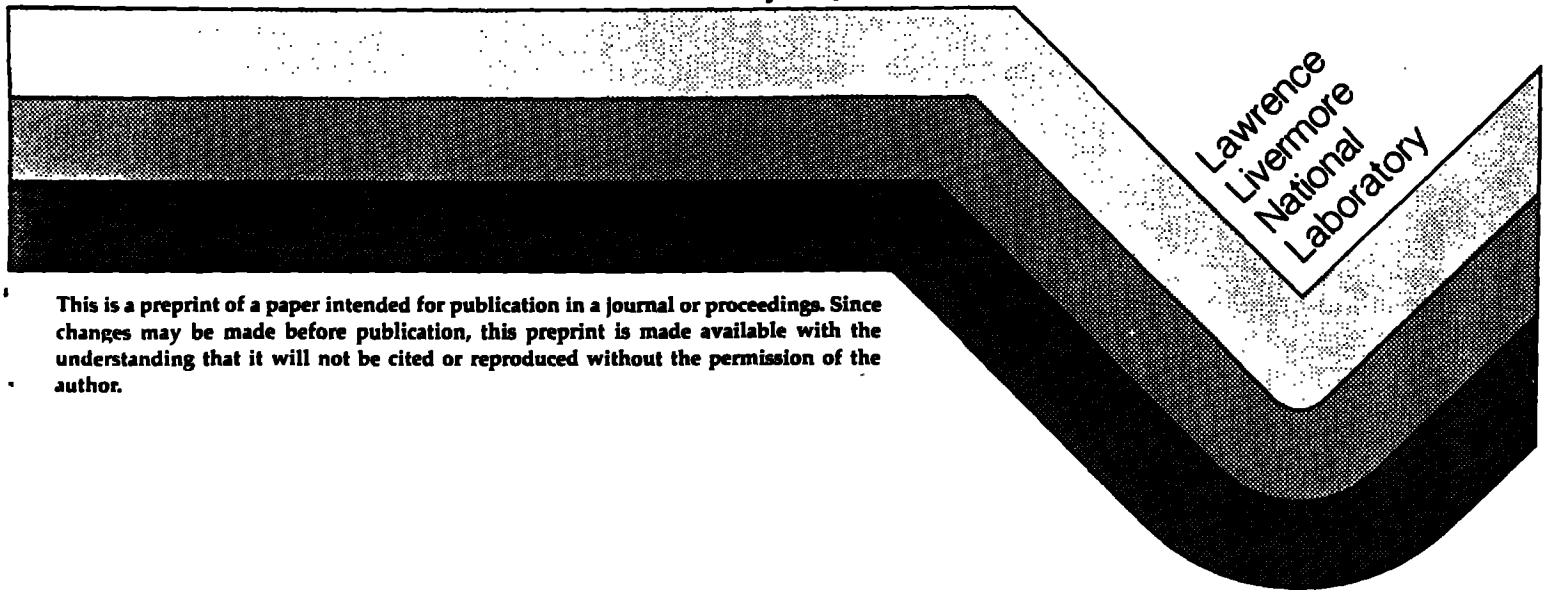

Work performed under the auspices of the U.S. Department of Energy by Lawrence Livermore National Laboratory under Contract W-7405-ENG-48.

# TIME-IMPLICIT SIMULATION OF PARTICLE-FLUID SYSTEMS

J. Denavit
Lawrence Livermore National Laboratory
P. O. Box 808, L-18
Livermore, California 94550

ABSTRACT. This paper presents one-dimensional particle-fluid hybrid simulations in which the strongly collisional components of the plasma (e.g., ions and thermal electrons with $\nu_{cf}\Delta t > 1$) are treated as fluids and the weakly collisional components (e.g., energetic electrons with $\nu_{cp}\Delta t << 1$) are treated as particles. Here $\nu_{cf}$ denotes the fluid ion and electron collision frequencies, $\nu_{cp}$ is the energetic particle collision frequency and $\Delta t$ is the time step. Collisions between particle and fluid components are treated by a Monte-Carlo method and mass transfers between the particle and fluid electron components are governed by collision frequency thresholds. The field is computed implicitly to allow time steps with $\omega_p \Delta t > 1$ ($\omega_p$: plasma frequency).

## 1. INTRODUCTION

Both particle and fluid simulations have proven to be powerful research tools in plasma physics, but have generally been applied to different problems. In particle simulations, a large number of charged particles, representing the plasma, are followed in their self fields. At each time step, the charge and current densities are computed from the particle positions and velocities, and the electromagnetic fields are evaluated using Maxwell's equations. The particles are then advanced, using these fields, over a time increment, $\Delta t$, and the process is repeated. This procedure is characterized as time-explicit because it uses known particle positions and velocities, at a time $t_o$, to compute the fields which are then used to advance the particles beyond this time, to $t > t_o$. Particle simulations give a very detailed description of the plasma, which is particularly useful in the study on non-equilibrium phenomena, where the distribution function exhibits multiple streaming, supra-thermal tails, or other non-Maxwellian features. However, they are generally limited to short time scales, of the order of the plasma period, $\omega_p^{-1}$, because the explicit nature of the algorithms used gives a violent numerical instability for time step sizes, $\Delta t > \omega_p^{-1}$. Here $\omega_p = (4\pi e^2 n_e/m_e)^{1/2}$

is the electron plasma frequency, $n_e$ is the electron density, -e is the electron charge, $m_e$ is the electron mass and Gaussian cgs units are used.

In fluid simulations, the plasma is usually represented as a single fluid by MHD equations. Quasi-neutrality is assumed and the currents are computed from a generalization of Ohm's law. The transport coefficients used in the fluid equations assume that the distribution function is close to Maxwellian, and exclude such features as multiple streaming or supra-thermal tails, for example. Fluid simulations of this type are not limited by the condition $\Delta t \ll \omega_p^{-1}$, and give a description of the plasma over much longer time and space scales than particle simulations. They play an important role to model experiments, with realistic geometrical and physical parameters. However, they assume that collisions, or other microscopic effects, maintain the plasma sufficiently near local thermodynamic equilibrium to guarantee their validity.

Recently, particle (and Vlasov) simulation methods, using a time-implicit procedure, have been developed to allow particle simulations, including electron inertia, with large time steps $\Delta t > \omega_p^{-1}$. In this procedure, the fields are predicted at time $t_1 = t_o + \Delta t$, <u>before</u> advancing the particles (or the distribution function) to this time level. The particles (or the distribution function) are then advanced from $t_o$ to $t_1$, using a weighted average of the fields at $t_1$, $t_o$ and earlier times. In the first time-implicit methods to be introduced [1, 2, 3], the fields are evaluated at the new time, $t_1$, using a subsidiary fluid representation of the electrons in terms of the continuity and momentum equations. This method, now known as the "moments" method, has been applied to one-dimensional electrostatic problems such as the two-stream instability, ion acoustic waves and plasma expansion into vacuum. It has also been used in two-dimensional electromagnetic simulations [4]. In another method, which was introduced subsequently, the fields at $t_1$ are evaluated directly in terms of a susceptibility tensor derived from the equations used to advance particles [5]. This "direct" method has been applied to one-dimensional electrostatic problems and to two-dimensional simulations with a static magnetic field [6]. Its application to electromagnetic problems has also been implemented [7].

Implicit particle simulations, using either the "moments" or the "direct" method allow time steps $\Delta t \gg \omega_p^{-1}$. They can represent accurately low-frequency electron inertia effects, such as trapping or acceleration of energetic electrons, while providing rapid damping of high-frequency plasma oscillations. However, these methods remain limited by the condition $\Delta t \ll (kv_{th})^{-1}$, which specifies that an electron near the thermal velocity, $v_{th}$, must not move across a large fraction of a characteristic wavelength, $\lambda = 2\pi/k$, during a time step. Taken together, the conditions $\omega_p \Delta t > 1$ and $kv_{th}\Delta t \ll 1$ imply $k\lambda_D \ll 1$, where $\lambda_D = v_{th}/\omega_p$ is the Debye length. Thus, implicit methods yield improved efficiency only in the case of <u>long wavelengths</u> or in <u>dense</u> and <u>cold</u> plasmas. However, dense and cold plasmas also have large collision frequencies $\nu_c$ and implicit codes operating in this regime must therefore allow time steps with $\nu_c \Delta t > 1$.

These scaling considerations lead to the concept of a hybrid formulation, in which the sparse and hot component, is represented as particles and satisfies the conditions $\omega_p\Delta t \ll 1$, $kv_{th}\Delta t \ll 1$ and $\nu_c\Delta t \ll 1$, while the dense and cold component is given a fluid representation and is characterized by $\omega_p\Delta t > 1$, $kv_{th}\Delta t \ll 1$ and $\nu_c\Delta t > 1$. The fluid representation considered here does not use MHD equations, but is based on separate electron and ion fluids, and includes electron inertia. An implicit determination of the fields generated by fluid electrons is therefore needed to achieve $\omega_p\Delta t > 1$ for this component.

The computations discussed in this paper are one dimensional. The fluid quantities are represented on a uniform Eulerian grid, which is also used for the particles, and flux corrected transport (FCT) is used to minimize numerical diffusion.

## 2. FLUID COMPONENTS

### 2.1 Fluid Equations

Since electron inertia is included, the electrons and ions are represented in terms of similar sets of fluid equations for conservation of mass, momentum and energy. This is a more elementary representation of the plasma than the MHD equations. It includes charge separation effects and, for example, the current density in this model is related to the electric field through the dynamics of the plasma components, rather than being computed from a generalization of Ohm's law.

The one-dimensional equations for a non-magnetized multi-species fluid are

$$\frac{\partial n_s}{\partial t} + \frac{\partial}{\partial x}(n_s u_s) = 0 \ , \tag{1}$$

$$\frac{\partial P_s}{\partial t} + \frac{\partial}{\partial x}(u_s P_s) = -\frac{1}{m_s}\frac{\partial p_s}{\partial x} + \frac{e_s}{m_s} n_s E + \frac{1}{m_s}\sum_{s'} R_{ss'} \tag{2}$$

$$\frac{\partial U_s}{\partial t} + u_s \frac{\partial U_s}{\partial x} = -\frac{1}{n_s} p_s \frac{\partial u_s}{\partial x} - \frac{1}{n_s}\frac{\partial q_s}{\partial x} + \frac{1}{n_s}\sum_{s'} Q_{ss'} \tag{3}$$

Here, $n_s$, $u_s$, and $T_s$ denote respectively the density, the drift velocity and the temperature of species s, $P_s = n_s u_s$ defines the momentum, E is the electric field, $m_s$ and $e_s$ are the mass and charge of the particles of species s. Monoatomic ideal gases are assumed with the pressure, $p_s = k_B n_s T_s$ and specific energy $U_s = (3/2)k_B T_s$, where $k_B$ denotes the Boltzmann constant.

The collisional friction force between components s and s' is given by

$$R_{ss'} = - m_{ss'} C_{ss'} n_s n_{s'} (u_s - u_{s'}) \tag{4}$$

where $m_{ss'} = m_s m_{s'}/(m_s + m_{s'})$, and $C_{ss'}$ is a collision parameter. For Coulomb collisions between charged particles, a generalization of Braginskii's results [8] gives

$$C_{ss'} = \frac{\alpha_o \Lambda_{ss'} e_s^2 e_{s'}^2}{(2\pi)^{3/2} \epsilon_o \sqrt{m_{ss'}} (k_B T_{ss'})^{3/2}} \tag{5}$$

where $\Lambda_{ss'}$ is the Coulomb logarithm, $\epsilon_o$ is the dielectric constant of free space and $T_{ss'} = m_{ss'}[(T_s/m_s) + (T_{s'}/m_{s'})]$. Note that all quantities entering in Eq. (4) are symmetrical with respect to s and s', giving $R_{ss'} + R_{s's} = 0$. The thermal gradient force is not considered here.

The heat transfer between species is due to both dissipation and temperature differences,

$$Q_{ss'} = - \frac{m_{ss'}}{m_s} R_{ss'} (u_s - u_{s'}) - 3 \frac{m_{ss'}}{m_s + m_{ss'}} C_{ss'} n_s n_{s'} k_B (T_s - T_{s'}) . \tag{6}$$

Finally, the heat flux is

$$q_s = - \kappa_s \frac{\partial T_s}{\partial x} , \tag{7}$$

with the heat conduction reciprocal (heat resistivity) equal to the sum of a collisionless contribution, $1/\kappa_{so}$, which gives the flux limit, and collisional contributions, $1/\kappa_{ss'}$,

$$\frac{1}{\kappa_s} = \frac{1}{\kappa_{so}} + \sum_{s'} \frac{1}{\kappa_{ss'}} . \tag{8}$$

The collisionless contribution is

$$\frac{1}{\kappa_{so}} = f_s \frac{m_s^{1/2} |\nabla T_s|}{n_s (k_B T_s)^{3/2}} ,$$

where $f_s$ is the flux limiter coefficient. For Coulomb collisions between particles, a generalization of Braginskii's results [8] gives

$$\frac{1}{\kappa_{ss'}} = \frac{m_s n_{s'} C_{ss'}}{\gamma_s n_s k_B^2 T_s}$$

The numerical constants $\alpha_o$, $\gamma_e$, and $\gamma_i$ are given in Ref. [8].

## 2.2 Transport Algorithm

The mass and momentum conservation equations, Eqs. (1) and (2) are both of the form

$$\frac{\partial \rho}{\partial t} + \frac{\partial}{\partial x}(u\rho) = S \ , \tag{9}$$

where $\rho$ is the transported density, u is the velocity, and S is a source term which is zero in the case of Eq. (1). For the Eulerian representation on a fixed mesh, which has been chosen here, the transport algorithm solving Eq. (9) must ensure numerical stability without introducing excessive diffusion. Flux corrected transport (FCT) algorithms are used for this purpose [9]. The system is divided into J-2 cells of length $\Delta x$, with two guard cells, cells 1 and J, laying outside the system as shown in Fig. 1. All quantities are defined at the cell centers and the values at the guard cells are set equal to their values at the adjacent boundary cell, e.g., $\rho_1 = \rho_2$, $\rho_J = \rho_{J-1}$, $u_1 = u_2$, $u_J = u_{J-1}$. This choice allows the transport algorithm to be applied uniformly to all physical cells ($j = 2, \ldots, J-1$) and yields emitting or absorbing boundary conditions depending on the sign of u at the boundary cells. In addition, the mass, (or charge), momentum and energy crossing the boundaries of the system are stored separately to allow conservation checks and to compute the electric field.

Following the FCT algorithm, provisional values, $\rho_j^{TD}$, of the density are first computed from the old values, $\rho_j$ and $u_j$,

$$\rho_j^{TD} = \frac{1}{2} Q_+^2 (\rho_{j+1} - \rho_j) - \frac{1}{2} Q_-^2 (\rho_j - \rho_{j-1}) + \rho_j (Q_+ + Q_-) \tag{10}$$

where

$$Q_\pm = \frac{\frac{1}{2} \mp c_j}{1 \pm (c_{j\pm1} - c_j)} \ , \tag{11}$$

and $c_j = u_j \Delta t / \Delta x$. The source term, S, is not included here and will be introduced when the momentum equations are considered. Equation (10) gives provisional values of the density, which are always positive for $|c_j| < 1/2$. However, these values include a large numerical diffusion and are therefore both transported and diffused (TD). The

diffusion is corrected by application of an antidiffusion step, which is limited so as not to cause new maxima or minima of the density. The simplest antidiffusion step, is defined by

$$\Delta^{TD}_{j+\frac{1}{2}} = \rho^{TD}_{j+1} - \rho^{TD}_{j}, \tag{12}$$

$$s^{TD}_{j+\frac{1}{2}} = \text{sign}\,(\Delta^{TD}_{j+\frac{1}{2}}), \tag{13}$$

$$\phi_{j+\frac{1}{2}} = s^{TD}_{j+\frac{1}{2}} \max\left\{0, \min\left[s^{TD}_{j+\frac{1}{2}}\,\Delta^{TD}_{j-\frac{1}{2}}, \frac{1}{8}\left|\Delta^{TD}_{j+\frac{1}{2}}\right|, s^{TD}_{j+\frac{1}{2}}\,\Delta^{TD}_{j+\frac{3}{2}}\right]\right\} \tag{14}$$

$$\rho^{new}_{j} = \rho^{TD}_{j} - (\phi_{j+\frac{1}{2}} - \phi_{j-\frac{1}{2}}) \quad , \tag{15}$$

where $\rho^{new}_j$ is the new density. This algorithm leaves a significant residual diffusion, even in the stationary case, and more advanced algorithms are given in Ref. [9].

## 2.3 Momentum Equations

The equation of continuity, Eq. (1), which has a right member equal to zero, may be solved by direct application of one of the FCT algorithms. However, Eq. (2) requires the computation of a source term S. In the implicit time step considered here, this source term is split into two parts. The first part, computed from the old values of the variables is applied before transport,

$$\bar{P}_{sj} = P_{sj} + F_{sj}\frac{\Delta t}{2} - \sum_{s'}(1-\theta_1)\Delta t\,\frac{m_{ss'}}{m_s}\,C_{ss'j}(n_{s'}P_s - n_s P_{s'}); \tag{16}$$

where

$$F_{sj}\frac{\Delta t}{2} = -\frac{\Delta t k_B}{4m_s\Delta x}[(nT)_{j+1} - (nT)_{j-1}]_s + \frac{e_s\Delta t}{2m_s}(n_s E)_j \ . \tag{17}$$

Here, j denotes the grid point, $\Delta x$ is the mesh size, and $\theta_1$ is a weight factor which allows the friction force to be either time centered ($\theta_1 = 1/2$) or implicit ($\theta_1 = 1$). The second part of the time step, computed from the new values is applied after transport. Since the new values are unknown, this partial step requires iterations. Let the superscripts q and q+1 denote successive iteration levels, then

$$P_{sj}^{q+1} = FCT(\bar{P}_s)_j + F_{sj}^q \frac{\Delta t}{2}$$

$$- \sum_{s'} \theta_1 \Delta t \frac{m_{ss'}}{m_s} C_{ss'j}(n_{s'}P_s - n_s P_{s'})_j^{q+1} \tag{18}$$

The friction force, which can be very large in dense fluids cannot be included in the iteration without causing divergence for $\nu_{cf}\Delta t > 1$, where $\nu_{cf}$ is the fluid collision frequency. Equations (18) must therefore be solved as a system of linear equations,

$$A_{ss'j} P_{s'j}^{q+1} = B_{sj} \tag{19}$$

where

$$A_{ss'j} = - \theta_1 \Delta t \frac{m_{ss'}}{m_s} C_{ss'j} n_s \tag{20}$$

for $s' \neq s$,

$$A_{ssj} = 1 - \sum_{s \neq s'} A_{ss'j} \, . \tag{21}$$

and

$$B_{sj} = FCT(P_s)_j + F_{sj}^q \frac{\Delta t}{2} \tag{22}$$

For $\omega_p \Delta t > 1$, the electric field which enters in Eq. (17), must also be evaluated implicitly, but this question is examined separately in Sec. 4.

## 2.4 Temperature Equations

Equation (3) for the temperature has different transport terms than the continuity and momentum equations, Eqs. (1) and (2). However, it can be rearranged to allow the electron and ion temperatures to be advanced using one of the FCT algorithms already used for mass and momentum transport,

$$\frac{3}{2} \left[\frac{\partial T_s}{\partial t} + \frac{\partial}{\partial x}(u_s T_s)\right] = w_s + r_s + d_s \tag{23}$$

where

$$w_s = \frac{1}{2} \frac{\partial u_s}{\partial x} T_s + \sum_{s'} \frac{m_{ss'}^2}{m_s} \frac{C_{ss'}}{k_B} n_{s'}(u_s - u_{s'})^2 \tag{24a}$$

is due to compression and dissipation,

$$r_s = -\sum_{s'} \frac{3m_{ss'}}{m_s+m_{s'}} C_{ss'} n_s (T_s - T_{s'}) \qquad (24b)$$

is due to temperature relaxation between components and

$$d_s = \frac{1}{n_s} \frac{\partial}{\partial x} \kappa_s \frac{\partial T_s}{\partial x} \qquad (24c)$$

is due to heat conduction.

The temperature is updated through a succession of partial steps:

i) Local temperature changes due to terms $w_s$ and $r_s$
ii) Heat diffusion
iii) Transport.

## 3. PARTICLE COMPONENT

The particles are generated from the corresponding fluid when the local collision frequency drops below a threshold $\nu_1$, and are re-absorbed into the fluid when their collision frequency becomes larger than another threshold, $\nu_2$. Thus a given region of space may be occupied either by fluids only, by particles only, or by a mixture of both components, which interact with each other by collisions and through the electric field. Since scattering of particles by the fluid components causes a rotation of their velocity, the particle variables for the one-dimensional, non-magnetized case, must include the position, x, and two velocity components, $v_x$ parallel to the x-axis and $v_t$ tranverse (i.e., perpendicular) to this axis.

Several methods have been used in particle simulations to relate the particles,which are located at discrete points $x_i$, where i designates a given particle, to the grid quantities, which are defined at the grid points (or cell centers), $x_j$. Among these methods, nearest grid point (NGP) is the simplest. In NGP, the charge of a particle contributes only to the cell in which it is located and the electric force is due only to the field at this cell center. In another method, area sharing, particles are considered to be sheets of finite thickness, $\Delta x$, equal to the cell size, and only the fraction of the particle located in a given cell contributes to the charge in this cell, with the remaining fraction contributing to the adjacent cell. The force in this case is computed by linear interpolation of the field at adjacent cell centers. Both methods conserve momentum but area sharing, which gives smoother fields and generates less noise, is generally favored over NGP. However, in the hybrid simulations considered here, consistency between particle and fluid components is easier to achieve with NGP.

The initial location of the particles must be such that the instantaneous electric field array is unchanged by the mass transfer from fluid to particles. The total electric force on the new particles must also be equal to the force on the fluid element they

replace. In the case of NGP, this can be achieved by locating the new particles anywhere within the cell, and in particular, they can be distributed uniformly within the cell. In the case of area sharing, the new particles must all be initialized at the cell centers. Any deviation from this location would spread their charge to the neighboring cells, and cause the electric force on these particles to be affected by neighboring values of the electric field. It follows that the initial distribution of particles is more discrete when area sharing is used than when NGP is used. This tends to cancel the advantages of area sharing over NGP in achieving low noise simulations.

Since strongly collisional particles are eliminated from the simulation by absorption into the fluid electron component, the particles can be assumed to satisfy the conditions $\nu_{cp}\Delta t << 1$. The particles can therefore be advanced using a split time step. Velocities and positions are advanced by a simple leap-frog scheme under the action of the electric field but under collisionsless conditions. This partial step is followed by a collisional step under field-free conditions. In the collisional step the particle velocity is decreased to account for energy loss by collisions with the fluid components and it is rotated to account for random scattering.

## 4. ELECTRIC FIELD

### 4.1 Implicit Algorithm

The electric field is evaluated from a finite difference approximation of Poisson's equation

$$G_j \equiv E_{j+1}^{t+\Delta t} - E_j^{t+\Delta t} - \frac{\Delta x}{2\epsilon_0}\left[\sum_s e_s (n_{j+1} + n_j)_s + \rho_{pj}\right] = 0 \qquad (25)$$

where $\rho$ is the charge density due to particles, and $j = 2, \ldots, J-2$. Recall that the system consists of cells 2 thru J-1, see Fig. 1, with cells 1 and J as guard cells, used only to satisfy boundary conditions in the transport algorithm.

The quantity $G_j$ may be considered as a multidimensional "vector" function, $\underline{G}(\underline{E}^{t+\Delta t})$ of the multidimensional "vector", $E_j^{t+\Delta t}$, both $\underline{G}$ and $\underline{E}^{t+\Delta t}$ having one component for each grid point $j = 2, \ldots, J-1$ in the system. Recall that since $j = 1$ and $j = J$ correspond to guard cells they do not contribute independent values of $E_j$ or $n_{sj}$. Equation (25) is solved using the well-known Newton iteration scheme. The $(q+1)$-th approximation of the field is written as the sum, $E_j^{q+1} = E_j^q + \delta E_j^{q+1}$ of the q-th approximation and a correction $\delta E_j^{q+1}$. Taylor expansion of Eq. (25)

$$G_j(\underline{E}^q + \delta\,\underline{E}^{q+1}) \simeq G_j(\underline{E}^q) + \sum_{j'} \left(\frac{\partial G_j}{\partial E_{j'}}\right)^q \delta E_{j'}^{q+1} = 0,$$

or

$$\sum_{j'} \left(\frac{\partial G_j}{\partial E_{j'}}\right)^q \delta E_{j'}^{q+1} = - G_j(\underline{E}^q) \quad . \tag{26}$$

This set of equations, with j = 2, ..., J-1, can be solved for the corrections $\delta E_j^{q+1}$ after the matrix $(\partial G_j/\partial E_{j'})^q$ and the vector $G_j(\underline{E}^q)$, which depend only on earlier approximations have been evaluated.

It is important note that the new electric field enters in the definition of $G_j$ in Eq. (25), not only in the explicit terms $E_j^{t+\Delta t}$ and $E_{j+1}^{t+\Delta t}$, but also implicitly through the densities $n_{sj}^{t+\Delta t}$ and $\rho_j^{t+\Delta t}$, since these quantites depend on the new electric field via the algorithms described in Sections 2 and 3. Recognition of this implicit dependence is essential to establish an iterative scheme which is convergent for $\omega_p \Delta t > 1$. Here, only the dependence of $G_j$ on $\underline{E}$ via the fluid densities $n_s$ is considered. The dependence of $G_j$ on $\underline{E}$ via the particle charge is computed as in implicit particle simulations [5].

From the transport algorithm, Eqs. (10) and (11), applied to the electron continuity equation,

$$Q_{\pm} = \frac{1}{2} [1 \mp (c_{j\pm1} - c_j)] \mp c_j + O(c^2) \ ,$$

and

$$n_{sj}^{t+\Delta t} = \frac{1}{4} (c_{j-1} + c_j)\, n_{sj-1} + [1 - \frac{1}{4} (c_{j+1} - c_{j-1})]\, n_{sj} - \frac{1}{4} (c_j + c_{j+1})\, n_{sj+1} \ , \tag{27}$$

where j = 2, ..., J-1. In Eq. (27), the nonlinear limitations to the antidiffusion step, given by max and min functions in Eq. (14) have been neglected.

From the fluid momentum equations, Eqs. (19)

$$p_{sj}^{q+1} = \sum_{s'} (A^{-1})_{ss'j} B_{s'j}$$

or

$$u_{sj}^{q+1} = \sum_{s'} (A^{-1})_{ss'j} \frac{e_{s'} \Delta t}{2m_{s'}} n_{sj} E_j^{q+1} + u_{sj}^*$$

where $u_{sj}^*$ denotes terms independent of $E^{q+1}$ to first order. Evaluating $c_j$ from this expression and substituting into Eqs. (27) and (25) gives

$$g_{j1} = \frac{\partial G_j}{\partial E_{j-1}} = - \sum_s e_s (n_{j-1} + n_j)_s\, Q_{sj-1} \ ,$$

$$\varepsilon_{j2} = \frac{\partial G_j}{\partial E_j} = -1 - \sum_s e_s (n_{j-1} + n_j)_s \, Q_{sj} \,,$$

$$\varepsilon_{j3} = \frac{\partial G_j}{\partial E_{j+1}} = 1 + \sum_s e_s (n_{j+1} + n_{j+2})_s \, Q_{sj+1} \,, \tag{28}$$

$$\varepsilon_{j4} = \frac{\partial G_j}{\partial E_{j+2}} = \sum_s e_s (n_{j+1} + n_{j+2})_s \, Q_{sj+2} \,,$$

where

$$Q_{sj} = \sum_{s'} \frac{e_{s'} \Delta t^2}{32 \epsilon_o m_{s'}} (A^{-1})_{ss'j} \,.$$

## 4.2 Electric Field Solution

The electric field corrections, $\delta E_j^{q+1}$, at grid points within the system, $j = 2, \ldots, J-1$, are obtained by solving Eqs. (26). The right members, $G_j$, are given by Eq. (25) and the matrix $\partial G_j / \partial E_j$, is given by Eqs. (28). For some problems, such as in the double layers, a fixed potential difference $\phi$ must be maintained across the system. In this case, the last of Eqs. (26), corresponding to $j = J-1$, must be disgarded and replaced by the equation

$$\sum_{j=1}^{J-1} \delta E_j^{q+1} = 0 \,, \tag{29}$$

which follows from the requirement that both $E_j^{q+1}$ and $E_j^q$ must satisfy the potential condition, $\sum_{j=2}^{J-1} E_j = -\phi/\Delta x$.

To solve this set of equations conveniently by means of a band matrix solver, Eqs. (26), with $j=2, \ldots, J-2$ are written in the form

$$\varepsilon_{22} \, \delta E_2 + \varepsilon_{23} \, \delta E_3 + \varepsilon_{24} \, \delta E_4 = -G_2 \,,$$

$$\varepsilon_{31} \, \delta E_2 + \varepsilon_{32} \, \delta E_3 + \varepsilon_{33} \, \delta E_4 + \varepsilon_{34} \, \delta E_5 = -G_3 \,,$$

$$\ldots\ldots$$

$$\varepsilon_{J-3,1} \delta E_{J-4} + \varepsilon_{J-3,2} \delta E_{J-3} + \varepsilon_{J-3,3} \delta E_{J-2} = -G_{J-3} - \varepsilon_{J-3,4} \delta E_{J-1} \,,$$

$$\varepsilon_{J-2,1} \, \delta E_{J-3} + \varepsilon_{J-2,2} \, \delta E_{J-2} = -G_{J-2} - \varepsilon_{J-2,3} \, \delta E_{J-1} \,.$$

This system is solved twice, first with $-G_2, \ldots, -G_{J-2}$ in the right members to obtain a set of partial corrections, $\delta E_j$, then with $0, \ldots, 0, -\varepsilon_{J-3,4}, -\varepsilon_{J-2,3}$ in the right members to obtain

a set of coefficients $C_j$. By superposition, the complete corrections are

$$\delta E_j = \delta \bar{E}_j + C_j \, \delta E_{J-1} \tag{30}$$

where j=2, ..., J-2, and $\delta E_{J-1}$ is unknown. To solve for $\delta E_{J-1}$, the $\delta E_j$'s from Eq. (30) are substituted into the potential condition, Eq. (29), from which

$$\delta E_{J-1} = - \frac{\delta \bar{E}_2 + \ldots + \delta \bar{E}_{J-2}}{C_2 + \ldots + C_{J-1}} \tag{31}$$

after which, $\delta E_2$, ... $\delta E_{J-2}$, are formed from Eq. (30).

## 5. EXAMPLES

The expansion of a plasma slab into vacuum is considered as an example. The slab is initially occupying a region of width 2L, located in the center of the simulation region of width 8L, where $L = 10^3 \lambda_{Do}$ is the characteristic length, $\lambda_{Do} = (T_o/4\pi e^2 n_o)^{1/2}$, $n_o$ is the characteristic density and $T_o$ is the characteristic temperature. The slab is initially represented as fluids only, defined in normalized units (see Table I) by setting $n_e = n_i = 1$, $u_e = u_i = 0$, $T_e = 1$, $T_i = 10^{-2}$. A mass ratio $m_i/m_e = 900$, and a charge number $Z_i = 1$ are assumed.

According to a similarity solution of this problem [10], which assumes charge neutrality, isothermal electrons and cold ions, the expansion produces a rarefaction wave, which propagates into the plasma at the ion acoustic speed $c_s = (T_e/m_i)^{1/2}$, equal to 1/30 in normalized units. Behind this wave, the electron and ion densities vary according to $n_e = n_i = n_o \exp[-(1 + x/c_s t)]$, where $n_o$ is the unperturbed density and x is measured from the location of the initial density discontinuity. The electrons and ions are accelerated outward according to the velocity profile $u_e = u_i = c_s + x/t$ and the electric field is uniform with a value $E = T_e/(c_s t)$, equal to 30/t in normalized units.

### CASE A: Collisionless, Isothermal Fluids Only

In this case, particle generation is turned off so that the simulation proceeds with fluids only, and a collisionless case is considered by setting $\alpha_o = 0$. In addition, the electron and ion temperatures are maintained constant ($T_e = 1$, $T_i = 10^{-2}$) throughout the computation. The electron density profile for this case is given in Fig. 2 at t = 4, 10 and 30, and the corresponding electric field profiles are shown in Fig. 3.

The propagation of the ion front predicted by the similarity solution is clearly visible on these profiles, and the fronts on each

side of the slab reach the center of the slab at t = 30, in agreement with the predicted speed, $c_s = 1/30$. At t = 30, the electric field on each side of the slab is $E = \pm 1$, in agreement with the expression $E = 30/t$ predicted by the similarity solution. At earlier times (t = 4 and 10) the field profiles also forms plateaus behind each rarefaction front, which are in approximate agreement with the expression $E = 30/t$, but large peaks are also observed. These peaks are due to the pure electron gas ahead of the ion front [11,12] and their magnitude is given approximately by $E_f \simeq 0.86\ (L/\lambda_{DO})(n_{ef}n_o)^{1/2}T_e$, where $n_{ef}$ the electron density at the front, which also coincides with the peak of the field. At t = 4, $n_{ef} \simeq 4 \times 10^{-4}$, see Fig. 2, yields $E_f = 17.2$, which is in approximate agreement with the simulation, $E_f = 19$, observed in Fig. 3. As time progresses, these peaks decrease, move outward (see Fig. 2 at t = 10) and disappear into the absorbing boundaries of the system.

In addition to the peaks, the field profile also exhibits oscillations which are primarily localized at the initial slab boundaries (x = 3 and x = 5). Since the plasma at these points move outward at the ion sound speed, it follows that the perturbation move relative to the plasma at the same speed and can therefore be interpreted as ion sound oscillations. Note that inward from the points x = 3 and x = 5, the plasma moves at a velocity which is less than $c_s$, thus allowing the ion-sound oscillations to propagate upstream.

The computations shown in Figs. 2 and 3 were done with three iterations of the electric field at each time step, and ran with a time step $\Delta t = 2 \times 10^{-3}$, which corresponds to $\omega_p \Delta t = 2$.

CASE B: Collisional Simulation with Fluids Only

The same plasma expansion problem is repeated using a full set of fluid equations, with $\alpha_o = 0.51$, $\gamma_e = 3.16$, $\gamma_i = 3.9$ and $C_{ei} = 1.92$. The results at t = 30, shown in Fig. 4, are qualitatively similar to the collisionless isothermal case. Note the scale on the electron temperature curve, $T_e$, in Fig. 4, showing that the electrons remain almost isothermal, but their temperature drops to $T_e \simeq 0.5$ as the slab expands. The ion temperature has increased an order of magnitude in the center of the slab but remains small in the expansion regions.

The energy of the electron fluid (kinetic plus thermal energies) is initially $W_e = 1.5\ n_e T_e \ell = 3$, where $n_e = 1$, $T_e = 1$ and $\ell = 2$ is the initial slab thickness. The ion fluid energy is initially $W_i = 0.03$ and the initial potential energy, $W_E$, is initially zero, giving a total energy $W_t = 3.03$. The time evolution of these quantities, given in Fig. 5, shows that (i) The electron energy drops steadily and is transferred to the ions, which eventually acquire an energy approximately equal to the electron energy. This is consistent with the increase in both ion velocity and ion temperature. (ii) The potential energy remains small $\sim 10^{-4}$ to $10^{-6}$, in agreement with the quasi-neutral evolution of the system and (iii) The total energy remains approximately constant out to t ≃ 15, when a significant amount of electron fluid reaches the boundaries of the system. The energy loss through both boundaries is $-W_e = [n_e u_e(u_e^2 + 3T_e)]_{xmax}$. For example,

at t = 20, the boundary values are $n_e = 1.5 \times 10^{-3}$, $u_e = 1.8$, and $T_e = 0.62$, from which $-W_e = 7.65 \times 10^{-3}$. This value agrees roughly with the slope of total energy curve in Fig. 5.

CASE C: Collisional Simulation with Particles

The plasma slab is again initialized with fluids only, with the same collisional parameters as in CASE B, but the particle thresholds are now set so that particles are generated when $\nu_e$ falls below $\nu_1 = 0.1$ and are absorbed when $\nu_{pe}$ is above $\nu_2 = 0.25$. In the interior of the plasma slab, $\nu_e = 1.9$, well above the generation threshold and the slab remains a fluid. However, as the electric field expands, the electron fluid elements ahead of the ion front, where $n_i = 0$, become collisionless. These fluid elements are changed into particles with a velocity distribution corresponding to the local values of $u_e$ and $T_e$. In the present simulation, the maximum particle weight is $w_{max} = 3 \times 10^{-4}$ and the minimum number of particles emitted is per cell is $N_{min} = 20$. After generation, these particles move self-consistently with the electron and ion fluids and form an energetic electron component which is trapped by the slab as shown in the phase plots of Fig. 6, for t = 0.4 and t = 4. The electric field profile, Fig. 7, is similar to the pure fluid cases, but the peaks are now higher, and the profile is noisier.

As the particles transit across the plasma slab, they lose energy by collisions and a fraction of them is re-absorbed into the fluid components as shown in the particle counts of Table II.

REFERENCES


1. T. L. Crystal, J. Denavit and C. E. Rathmann, Comments Plasma Phys. 5 (1979), 17.
2. J. Denavit and J. M. Walsh, in "Proceedings of the Ninth Conference on Numerical Simulation of Plasmas" Northwestern University, June 1980, paper PC3. Also, J. Denavit, J. Comput. Phys. 42 (1981) p. 337.
3. R. J. Mason, Los Alamos Scientific Laboratory Report LA-UR-80-2171, August 1, 1980. Also R. J. Mason, J. Comput. Phys. 41, (1981) p. 233.
4. J. U. Brackbill and D. W. Forslund, J. Comp. Phys. 46 (1982), 271.
5. A. Friedman, A. B. Langdon and B. I. Cohen, Comments Plasma Phys. 6, (1981) 225; A. B. Langdon, B. I. Cohen and A. Friedman, J. Comp. Phys. 51 (1983).
6. D. C. Barnes, T. Kamimura, J-N. Leboeuf and T. Tajima, J. Comp. Phys. 52 (1983), p. 480.
7. D. W. Hewett and A. B. Langdon, Laser Program Annual Report-1984, Lawrence Livermore National Laboratory, Livermore, CA.
8. S. I. Braginskii, in "Reviews of Plasma Physics" edited by M. A. Leontovich, Vol. 1, Consultant Bureau, N.Y. (1965) pp. 203-311.
9. J. P. Boris and D. L. Book, J. Comp. Phys. 11 (1973), 38 and 20 (1976), 397. D. L. Book, J. P. Boris and K. Hair, J. Comp. Phys. 18 (1975), 248.

10. J. E. Allen and J. G. Andrews, J. Plasma Phys. 4 (1970), 187.
11. J. E. Crow, P. L. Auer and J. E. Allen, J. Plasma Phys. 14 (1975), 65.
12. J. Denavit, Phys. Fluids 22 (1979), 1384.

*Work performed under the auspices of the U.S. Department of Energy by Lawrence Livermore National Laboratory under contract #W-7405-Eng-48.

TABLE I. Units used to define normalized quantities.

| Quantity | Unit |
|---|---|
| Length | L (characteristic length) |
| Velocity | $v_o = (T_o/m_e)^{1/2}$ (electron thermal velocity corresponding to characteristic temperature $T_o$) |
| Time | $t_o = L/v_o$ |
| Density | $n_o$ (characteristic density) |
| Electric Potential | $T_o/e$ |
| Electric Field | $T_o/eL = m_e v_o^2/eL$ |

TABLE II. Particle count for plasma expansion into vacuum, Case C.

| t | # Emitted | # Absorbed | # Net |
|---|---|---|---|
| 0 | 0 | 0 | 1 |
| 0.4 | 2480 | 744 | 1737 |
| 0.8 | 5520 | 1763 | 3758 |
| 1.2 | 11700 | 4006 | 7695 |
| 1.6 | 21580 | 7173 | 14408 |
| 2.0 | 35720 | 11559 | 24162 |

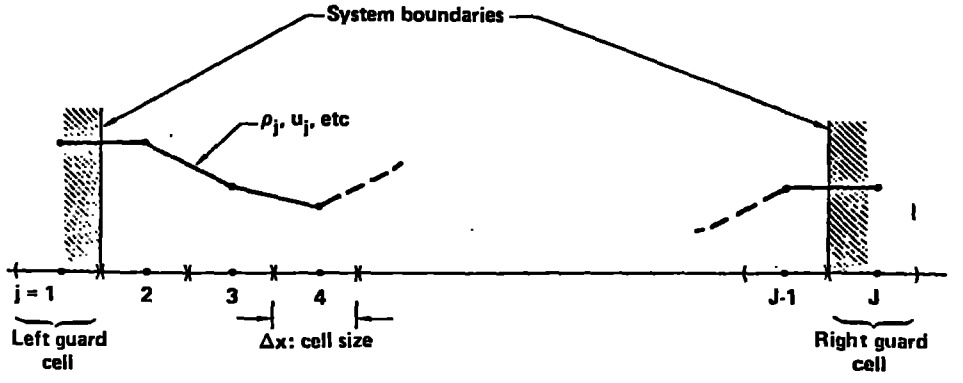


Fig. 1: Uniform Eulerian grid used to represent fluid and particle quantities.

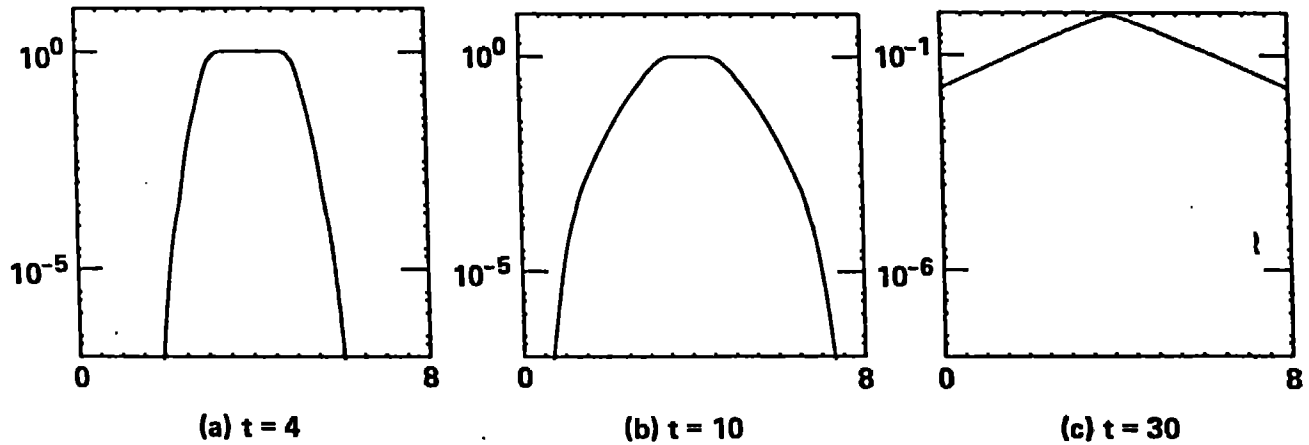


**Fig. 2: Ion density for collisionless, isothermal plasma slab expansion into vacuum with fluids only (CASE A).**

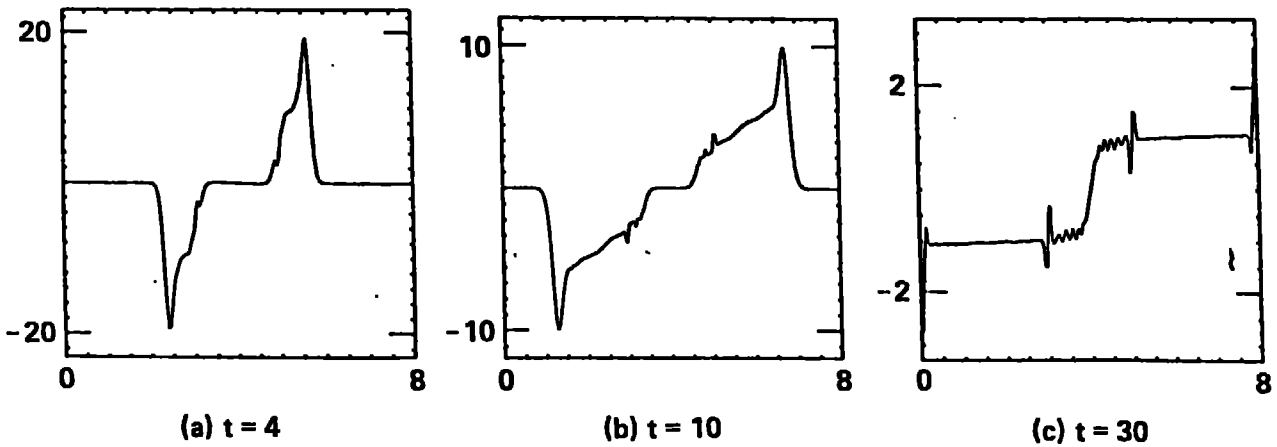


**Fig. 3: Electric field for CASE A.**

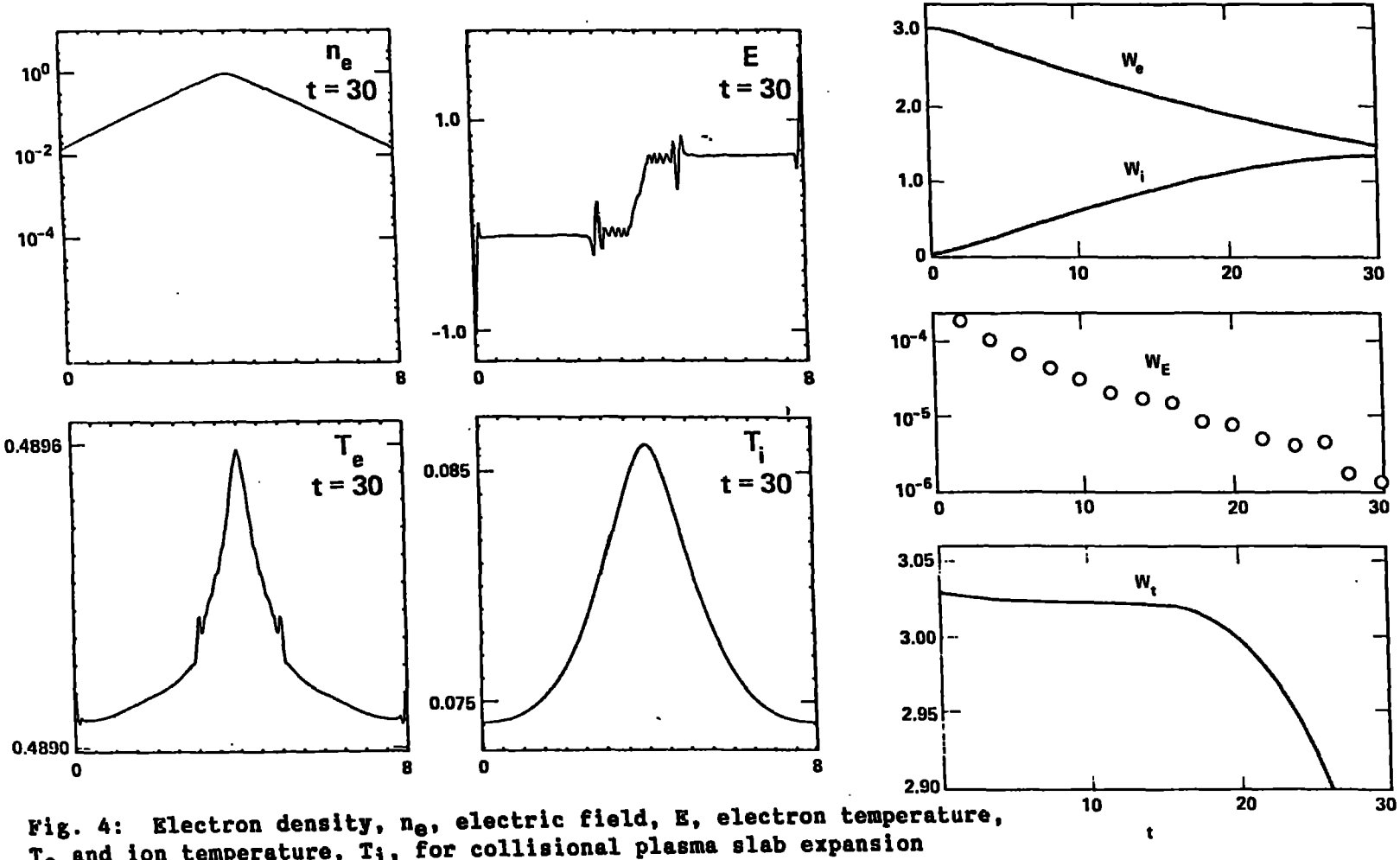


Fig. 4: Electron density, $n_e$, electric field, E, electron temperature, $T_e$ and ion temperature, $T_i$, for collisional plasma slab expansion into vacuum with fluids only (CASE B).

Fig. 5: Electron kinetic energy, $W_e$, ion kinetic energy, $W_i$, potential energy, $W_E$ and total energy as a function of time for CASE B.

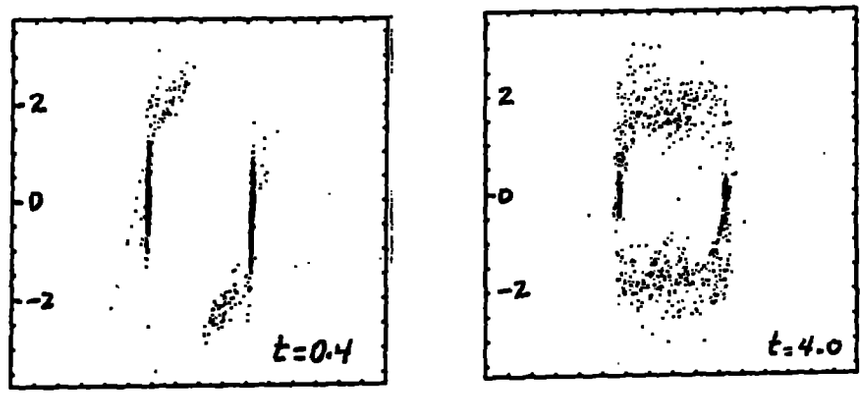


Fig. 6: Electron particle phase plot for plasma slab expansion into vacuum (CASE C).

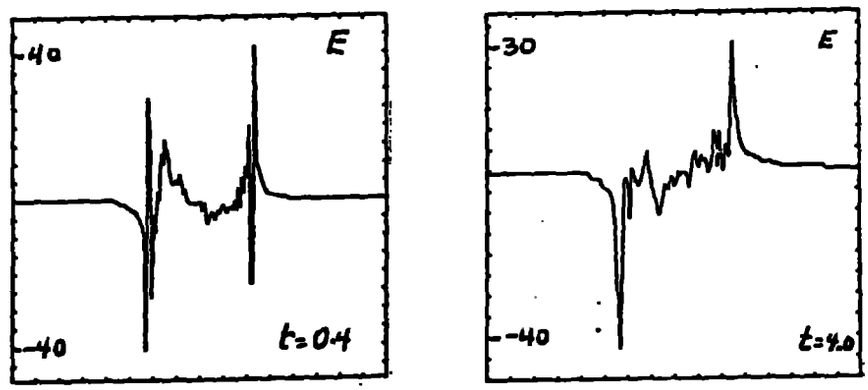


Fig. 7: Electric field for CASE C.